AGU PUBLICATIONS

Geophysical Research Letters

RESEARCH LETTER
10.1002/2014GL060073

Key Points:
- Long-duration (2000–2012) seismic array study of Southern Ocean noise sources
- Three *P* wave sources dominate: South Atlantic, Kerguelen, and Philippine Sea
- Noise sources show strong seasonality and slight interannual variability

Supporting Information:
- Readme
- Text S1
- Figure S1
- Figure S2
- Figure S3a
- Figure S3b

Correspondence to:
A. M. Reading,
anya.reading@utas.edu.au

Citation:
Reading, A. M., K. D. Koper, M. Gal, L. S. Graham, H. Tkalčić, and M. A. Hemer (2014), Dominant seismic noise sources in the Southern Ocean and West Pacific, 2000–2012, recorded at the Warramunga Seismic Array, Australia, *Geophys. Res. Lett.*, *41*, 3455–3463, doi:10.1002/2014GL060073.

Received 3 APR 2014
Accepted 8 MAY 2014
Accepted article online 13 MAY 2014
Published online 28 MAY 2014

Dominant seismic noise sources in the Southern Ocean and West Pacific, 2000–2012, recorded at the Warramunga Seismic Array, Australia

Anya M. Reading[1], Keith D. Koper[2], Martin Gal[1], Leon S. Graham[1], Hrvoje Tkalčić[3], and Mark A. Hemer[4]

[1]School of Physical Sciences (Earth Sciences) and CODES Centre of Excellence in Ore Deposits, University of Tasmania, Hobart, Tasmania, Australia, [2]Department of Geology and Geophysics, University of Utah, Salt Lake City, Utah, USA, [3]Research School of Earth Sciences, Australian National University, Acton, ACT, Australia, [4]Centre for Australian Weather and Climate Research, CSIRO Marine and Atmospheric Research, Hobart, Tasmania, Australia

Abstract Seismic noise is important in determining Earth structure and also provides an insight into ocean wave patterns and long-term trends in storm activity and global climate. We present a long-duration study of seismic noise focused on the Southern Ocean using recordings from the Warramunga Seismic Array, Northern Territory, Australia. Using high-resolution analysis, we determine the seismic slowness and back azimuth of observed seismic noise, microseisms, at hourly intervals through over a decade (2000–2012). We identify three dominant sources of body wave (*P*) noise in the Southern Ocean which we interpret to originate from a South Atlantic source propagating as *PP* waves, and Kerguelen Island and Philippine Sea sources propagating as *P* waves. We also identify surface waves from around the Australian coast. All sources show distinct seasonality and a low, but discernable, interannual variability.

1. Introduction

Seismic noise, also known as ambient energy, and as microseisms, is the term given to the background signal observed continuously, at relatively low, fluctuating amplitudes, on seismic stations worldwide. These stations were originally intended for the recording of higher-amplitude transient signals from earthquakes or man-made explosions. As most seismic stations record continuously, a wealth of archival data exists for seismic noise analysis. A spectral analysis of seismic noise [*Aster et al.*, 2010; *Berger et al.*, 2004; *Stutzmann et al.*, 2000] reveals two distinct peaks in power spectral density at periods of approximately 14 s (primary microseisms, PM) and 7 s (secondary microseisms). The source of these peaks may be traced to excitation pathways with ocean sources, direct pressure on the seafloor and standing waves from the interaction of incident and reflected waves in the deep ocean [*Cessaro*, 1994]. The frequency doubling effect for the latter case, secondary microseisms, is responsible for their commonly used alternative name: double frequency (DF) microseisms. The connection between ocean storm activity and "hum," lower frequency seismic noise [*Rhie and Romanowicz*, 2006], has been established, and a large data set from USArray has been used in the analysis of hum, PM, and DF microseisms over a whole year [*Traer et al.*, 2012].

Seismic noise sources have a dual significance to the global geophysical community. First, as a source of energy for earth structure determination [*Harmon et al.*, 2010; *Poli et al.*, 2012; *Prieto et al.*, 2009; *Romanowicz*, 2008; *Tkalčić et al.*, 2012; *Zhang et al.*, 2010]. Such analysis techniques have become popular following the realization that Rayleigh waves may be extracted from ambient seismic noise, and the dispersion properties used to model the seismic structure [*Campillo and Paul*, 2003; *Shapiro and Campillo*, 2004]. An improved understanding of the location and variability of dominant sources will enable optimization of Earth structure studies that use this ambient seismic noise. Seismic noise has a second significance as it provides a strong indication of storm activity in the deep ocean. Deep ocean storm activity is of global interest owing to its role in the uptake of atmospheric CO_2 [*Canadell et al.*, 2007; *Le Quere et al.*, 2009]. The variability of CO_2 uptake under different storm conditions [*Gruber et al.*, 2009] is one reason for concern regarding the changing storminess of the Southern Ocean and its investigation using both in situ waverider buoy observations and satellite data [*Hemer*, 2010; *Hemer et al.*, 2010; *Young et al.*, 2011]. The seismic noise record has the potential to provide an independent data stream to monitor Southern Ocean storm activity [*Aster et al.*, 2010; *Stutzmann et al.*, 2009]. In this data-poor region, additional evidence may aid the future resolution of the apparent discrepancy

between the interpreted weakening of the Southern Ocean CO_2 uptake [*Le Quere et al*., 2007] and the observational Argo ocean data which display little evidence of this [*Boning et al*., 2008].

Notable previous observational seismology studies that have focused on the source of ocean microseisms include the identification of the source of *P*, *PP*, *PKP*, and core phases and analysis of the seismic wavefield in detail, over one or two calendar years [*Gerstoft et al*., 2008; *Hillers et al*., 2012; *Koper et al*., 2009, 2010; *Landès et al*., 2010]. Modeling studies provide complementary insights into the mechanism of noise generation and transmission of seismic energy from the ocean to the solid Earth [*Ardhuin et al*., 2011; *Hasselmann*, 1963; *Longuet-Higgins*, 1950]. The relationship between wave height and the amplitude of the associated microseisms is far from simple, with moderate sea states being known to generate high-amplitude noise [*Obrebski et al*., 2012]. The strong influence of the depth of the water column understood from modeling work has been confirmed by observational seismology studies [*Euler et al*., 2014].

The previous observational seismology work on deep ocean seismic sources, summarized above, encompasses long-duration studies using single stations, and studies of shorter duration that use seismic array data recorded in the Northern Hemisphere, with an emphasis on the study of Northern Hemisphere sources. We present a long-duration study (over a decade) using array seismic data recorded in the Southern Hemisphere, with a focus on noise from the Southern Ocean. We aim to inform Earth structure studies that use seismic noise and to gain an understanding of the location and seasonal and interannual variability of the dominant seismic noise sources in the Southern Ocean and West Pacific.

2. Data and Analysis

We analyze over a decade (20002012) of data from the Warramunga Seismic Array (WRA), located in inland Australia. This is a roughly L-shaped array, with irregular interstation separations of 2–3 km and a cluster of stations near the intersection of the two arms of the array. The WRA response function is given in Figure S1 in the supporting information. Our analysis focuses on a long time span of recorded data, and hence, we confine our analysis to the vertical components; however, some of the array elements are now three-component. During the years 2006, 2007, and 2009, there are some time intervals when the data recovery for WRA was incomplete due to technical challenges at this remote location. Therefore, we omit these years from our analysis to maintain the comparison of broadscale seasonal variation and interannual variability. Our general results are therefore based on 10 years of analysis.

Using a new implementation of a high-resolution approach (outlined in the supporting information) based on the Capon method [*Capon*, 1969; *Kvaerna and Ringdal*, 1986; *Kvaerna and Doornbos*, 1986], we identify the slowness and back azimuth of incoming waves using 1 h time windows, every hour, between January 2000 and December 2012. The new implementation uses an incoherently averaged signal (IAS) approach with temporal averaging [*Wax et al*., 1984] and includes diagonal loading of the cross-power spectral density [*Featherstone*, 1997] and is referred to subsequently as "IAS Capon." Each 1 h segment is divided into 23 nonoverlapping, temporal subwindows. The cross-power spectral density is calculated as an average of these subwindows for improved stability, and the projection frequency is set to the middle of the frequency range of interest (0.508 Hz, examples given in Figures S1a and S1b). Data input routines from an open source library are used [*Beyreuther et al*., 2010]. We also calculated the same parameters using a standard *fk* (frequency-wave number) approach [*Lacoss et al*., 1969] and a previously used Capon approach [*Capon*, 1969; *Koper et al*., 2009] to verify that the new computational procedures yield consistent results.

For each hour between 2000 and 2012, we estimate and extract the location of the dominant *P* wave and dominant surface wave energy, on a 0.5×0.5 s/° grid, provided the source is above the threshold of -2 dB signal strength. Earthquakes are included but mostly have a negligible effect on the summary plots as they are infrequent in comparison to the "hit count" for each grid cell for the seismic noise. Great earthquakes with a very large number of aftershocks are an exception but are readily distinguished from noise through their much more confined location in comparison to noise sources. In this study, the aftershocks due to the 11 March 2011 earthquake located near the east coast of Honshu, Japan, are excluded from the summary plots. The aftershocks due to the 26 December 2004 earthquake located off the west coast of northern Sumatra are not significant on the summary plot (They are visible on the relevant quarterly plots.). These data points are accumulated for the whole time span of the study (Figure 1), and are also accumulated in 3 month quarter year intervals, for each year with a complete data return (Figures S3a and S3b).

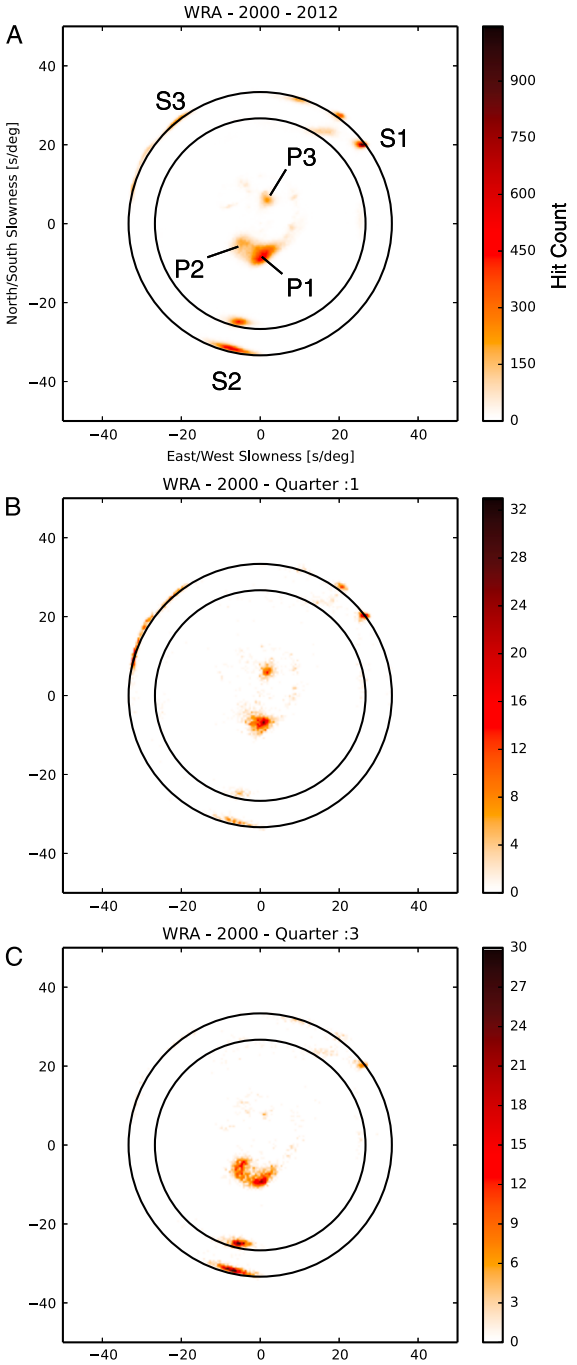

Figure 1. Summary plots showing dominant slowness and back azimuth of incoming seismic signals at Warramunga Seismic Array (WRA). (a) All seasons through all years 2000–2012 (2006, 2007, and 2009 were omitted due to intermittent data recovery; also omitted are the numerous aftershocks related to the 11 March 2011 "Tohoku" earthquake located near the east coast of Honshu, Japan). (b) Quarter 1, Northern Hemisphere winter (January–March), and (c) Quarter 3, Southern Hemisphere winter (July–September). Quarterly plots for all years are given in the supporting information (Figures S3a and S3b). P1, P2, and P3 indicate *P* wave arrivals discussed in the text. S1, S2, and S3 indicate surface wave arrivals (higher mode) discussed in the text. The outer circle indicates a slowness of 3.3 km/s (indicative of R_g waves), and the inner circle indicates a slowness of 4.16 km/s (indicative of L_g waves).

3. Dominant Noise and Seasonal and Interannual Variability

Summary plots which provide an overview of the typical pattern of incoming seismic signals are shown for the entire decade (2000–2012) and two quarters (i.e., seasons) of the year 2000 (Figure 1). Multiple extended sources, indicating regions that repeatedly give rise to surface and body wave energy, are observed in the summary plots. In this analysis, we focus on the highest hit count sources, i.e., those that correspond to the dominant source regions. The numerous sources of surface wave energy fall into three groups from each of which we select the most dominant source for analysis (S1, S2, and S3). Three dominant body wave sources (P1, P2, and P3) are identified for further investigation.

As an indication into the origin of the body wave sources, we show an example of the backprojected seismic noise location, for a single hour, superimposed on the ocean wave height model for the same time period (Figure 2). The slowness is estimated using the IAS Capon method (output shown in Figure S1c), backprojections make use of the global seismic structure reference model ak135 [*Kennett et al.*, 1995], and the wave heights are extracted from a long-duration hindcast model produced using the WAVEWATCH III model forced by Climate Forecast System Reanalysis winds [*Durrant et al.*, 2013].

Surface wave energy is consistent with R_g sources (guided, higher-mode Rayleigh waves) originating at the northeast margin of Australia (Figure 3, S1) and the far north of the west coast of Australia (S3). The strong source from a direction west of south, S2, corresponds to the Great Australian Bight (S2). This source produces dominant surface wave energy as both R_g and L_g (a relatively short-period phase, frequently observed for continental source-receiver paths, understood to propagate through predominantly transverse motion) which are clearly separated using the improved IAS Capon implementation (supporting information). The dominance of R_g on the array analysis of vertical component data is well

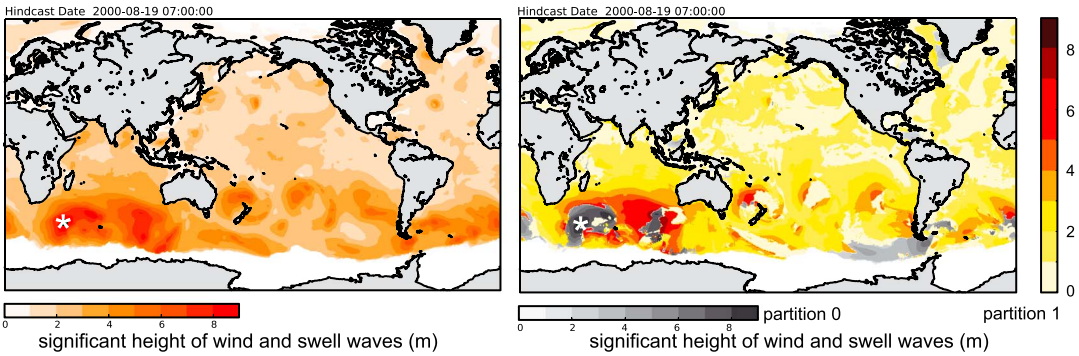

Figure 2. Plots showing the backprojected location (white star) of seismic noise clearly arriving as a *P* wave (2000:232:07 or 19 August). Significant wave height for the same time frame is shown, extracted from a hindcast model [*Durrant et al.*, 2013] together with the same model from two partitions. The partitions represent different domains in the spectral content of the wave height hindcast and are broadly indicative of opposing swell directions [*Hanson et al.*, 2009]. Locations where the right-hand plot shows dark red and dark grey patches overlapping are likely to generate the highest amplitude waves. The slowness estimation plot is provided (Figures S1c).

understood, and the clear appearance of L_g waves can be rationalized (including some vertical component particle motion) as indicative of second and higher modes of Rayleigh wave propagation. These modes include *SV*, vertically polarized *S* waves [*Ewing et al.*, 1957].

After backprojecting the body wave sources, we find that the most pervasive *P* wave source, P1, backprojects beneath the Antarctic continent, but a *PP* backprojection points to a South Atlantic noise source (Figure 4a). The second *P* wave source, P2, which is dominant for a lower proportion of the time, backprojects as *P* wave energy to the west of the Kerguelen Islands (Figure 4b). Source P3 backprojects as *P* wave energy to an area between the Philippine Sea and the Pacific Ocean margin near Japan (Figure 4c).

4. Seasonal and Interannual Variability

The general pattern of seasonal variation in hit count for each source region is shown by quarterly plots (Figures 1b and 1c). The seasonal variability in source strength for each individual year is also shown (Figure 5). The 3-D graphs show a three-class categorization of each source (strong, moderate, or weak/absent) for each quarter in each year which is broadly representative of the dominant incoming signals "seen" by the array. These classes were identified by a human analyst as representative of the signal characteristic for each source, for that quarter (Figures S3a and 3b). Alternate plots which source strength as both a categorized time series and as a continuous time series are provided (Figures S2a–S2c). The seasonal pattern suggested in

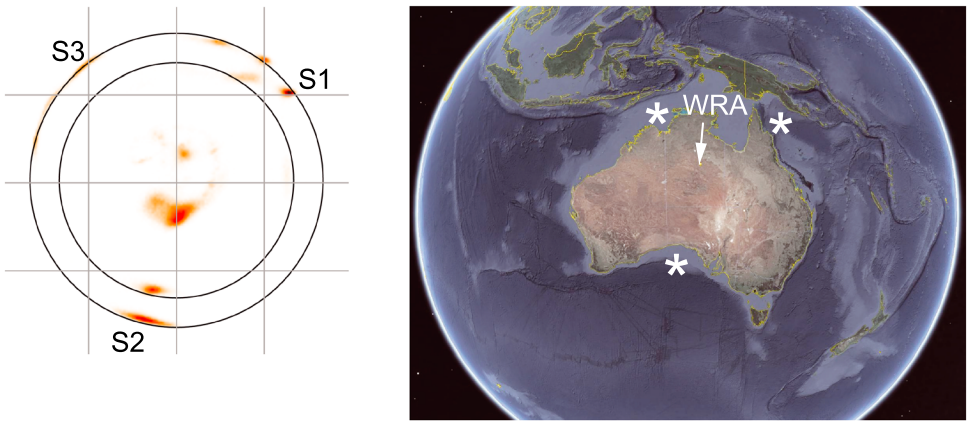

Figure 3. Interpreted source locations of dominant surface wave (higher-mode) sources. S1, S2, and S3 all have ray parameters close to the value of 3 km/s (R_g) shown by the outer circle. They are likely to arise at the continental shelf boundary at the locations shown. Base map from *Google Earth* [2013].

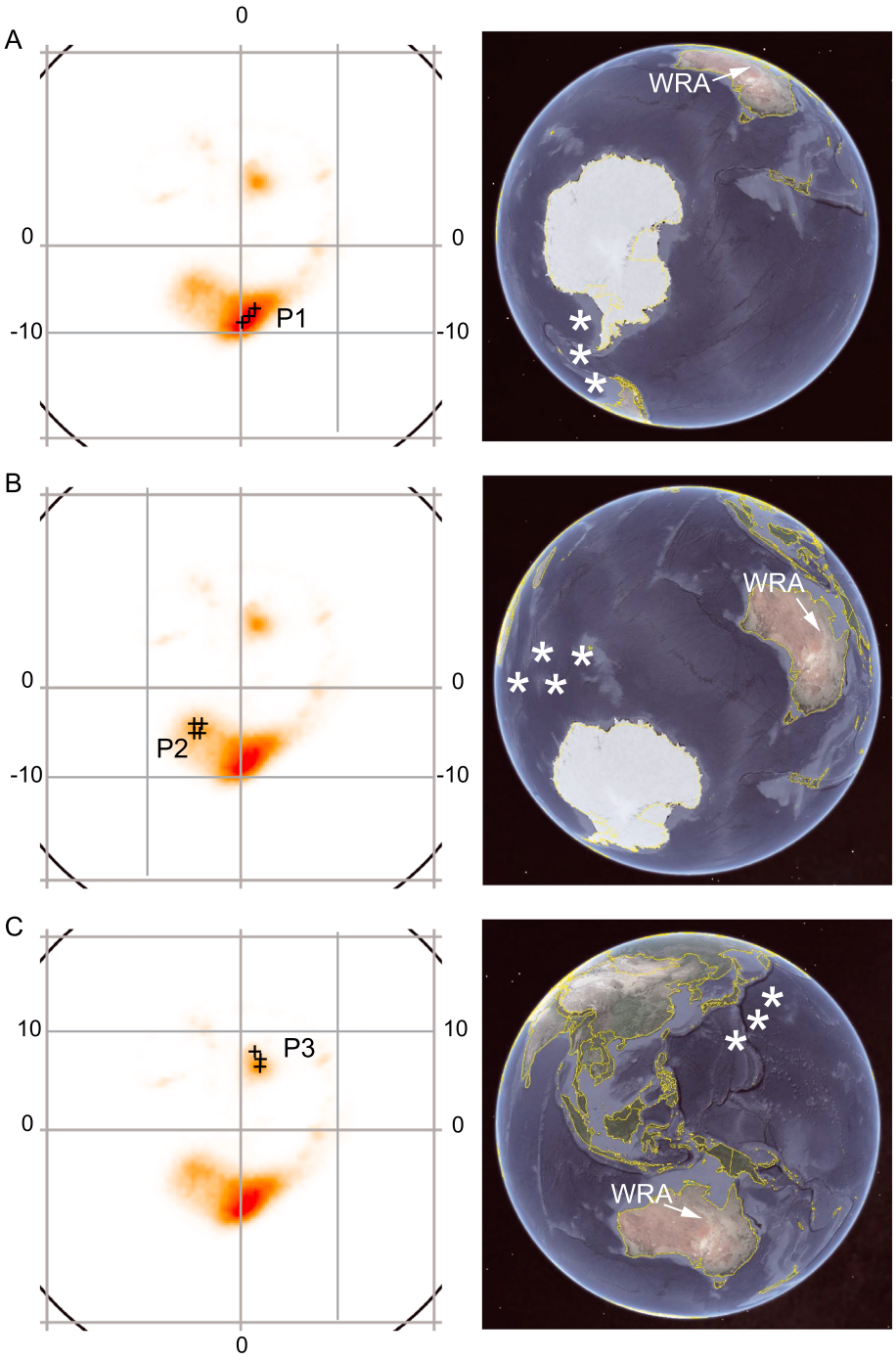

Figure 4. Interpreted source locations of dominant *P* wave sources. Plots in the left-hand column show an enlargement of Figure 1a. Crosses in left-hand column plots match to backprojected locations in the right-hand plots. WRA = Warramunga Seismic Array. (a) The strongest *P* wave source, P1, matches well to *PP* arrivals backprojected to the South Atlantic. (b) P2, which is highly seasonal with strongest arrivals in Q3 (Southern Hemisphere winter) matches to *P* arrivals backprojected to the region west of the Kerguelen plateau. (c) P3, a distinct set of *P* arrivals with strongest signals in Q1 and Q4 (Northern Hemisphere winter and spring) backprojects to the Philippine Sea and the region offshore of Japan. Base maps from *Google Earth* [2013].

the quarterly plots for 2000 (Figure 1) is shown to be a robust generalization. Body wave source P1 and surface wave source S1 are strong year round. For source P1, some years show a slight reduction in strength in Q2 (quarter 2, Southern Hemisphere autumn, April–June), and for S1 there is a slight reduction in strength in Q3 (southern winter, July–Sept). During Q1 (Northern Hemisphere winter), source P3 is strong;

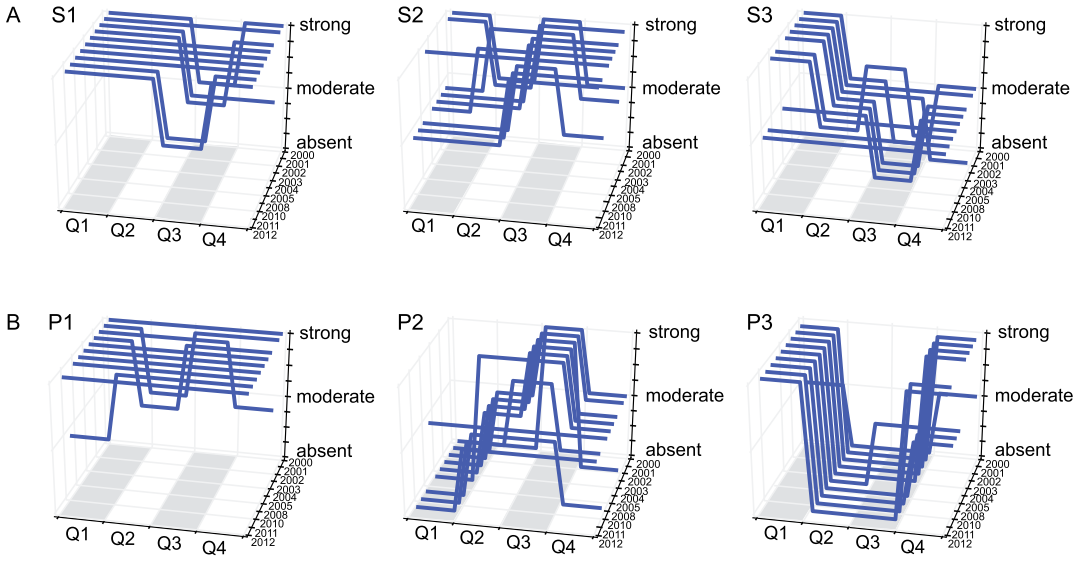

Figure 5. Summary plots showing the seasonal variation of dominant noise sources recorded at WRA for 10 individual years from 2000 to 2012 (omitting 2006, 2007, and 2009 as previously noted). The quarterly plots on which this summary is based are shown for all years in the supporting information (Figures S3a and S3b). (a) *S* wave sources as indicated in Figure 1: (b) *P* wave sources as indicated in Figure 1. The strength of each noise source for Quarter 1 (Q1: Northern Hemisphere winter, January–March) is indicated by the height of the bar at the left of each individual plot. Hence, P3 (Philippine Sea) is strong in Q1 and Q4, the northern winter and autumn. In contrast, P2 (Kerguelen) is strong in Q3, the Southern Hemisphere winter, July–September. P1 (South Atlantic) is strong year round with some years showing a slight reduction in strength in Q2, the Southern Hemisphere autumn, April–June. The patterns of surface wave energy show similar seasonality.

in contrast, sources P2 and S2 are strongest during Q3 (Southern Hemisphere winter). Source S3 is strongest during the summer (Q1), which is logical for this tropical latitude.

Interannual variability of the observed, dominant sources is low but discernable. Based on the 10 years analyzed in this study, a departure from typical seasonal patterns is indicated for each source for about 2 years in 10 (Figures 5 and S2). Such departures are one class removed from the general trend (i.e., a strong source showing as moderate, or moderate source showing as absent). Examples are years 2002 and 2010 when source P2 was absent (rather than moderate) in Q4. As further years of data become available, this preliminary result will be refined.

5. Discussion

We first consider estimation uncertainty and other aspects of the analysis methods, followed by a discussion of the implications of our interpretations (i) in using seismic noise in Earth structure determinations and (ii) in using seismic array methods to contribute to the understanding of the Southern Ocean and West Pacific wave climate.

The IAS Capon method improves the accuracy of the slowness estimation and also improves the yield of slowness and back azimuth estimates of noise sources from seismic array data when compared to standard Capon analysis (Figure S1). There are two reasons for this improvement in yield, first, refining the appearance of the most dominant sources, which enables two adjacent sources to be separated (e.g., the separation of R_g and L_g sources, Figure 3, source S2). Second, a lower amplitude source (or multiple sources) can be better identified in the presence of a higher-amplitude dominant source (we identify both a *P* and a surface wave noise arrival for the majority of the 1 h time windows).

The uncertainty in the slowness values that we estimate from the summary plots is effectively 0.5 s/° which results in a projected location uncertainty of ± 250 km for a noise source determination in a single hour. Noise sources due to ocean storms generally have a greater spatial extent than this value (note the extent of the dark patches close to the white stars in Figure 2); hence, the uncertainties due to the relatively small array aperture of WRA, the finite number of array elements, and uncertainty variability with direction due to the

orientation of the arms of WRA (Figure S1d) are not significant in the discussion that follows. The uncertainty in backprojection of the *P* wave sources is the most significant source of potential error; again, given the broad geographic extent of the noise sources as noted above, this is not a serious limitation when considering the general patterns of dominant noise. The typical range of slowness values in the high hit count regions (see Figure 4c, source P3) of the cross-power spectral density plots (2.5 s/°) maps to a range of almost 3000 km in source location, as indicated by the region spanned by the white stars in Figure 4.

With regard to the use of noise sources to determine structure, we first consider the dominant surface wave sources. *P* wave sources, relevant to studies of both global structure and wave climate, are then considered. The source of R_g surface waves (S1 and S3), which may be used for ambient seismic tomography determinations of structure, could be anywhere along the backprojected paths; hence, the source location at the continental shelf edge is not firmly constrained. The source of S2, with its accompanying L_g waves, is likely to be the edge of the continental shelf in the Great Australian Bight, as L_g waves do not propagate through oceanic crust [*Ewing et al*., 1957]. We note that as we are considering only the dominant surface wave source in each hour, attenuated L_g waves (e.g., from S1 and S3) may be evident from more detailed analysis of multiple sources. The orientation and station configuration of WRA, and consequently the lobes in its array response function (Figure S1d), may be slightly enhancing arrivals from the direction of S2.

The seasonality evident in sources S2 and S3 (Figures 1b, 1c, and 5a) implies that ambient seismic data including Quarter 3 (when S2 on the south coast is strongest) and Quarter 1 (when both S1 and S3 on the north coast are strong) should be included in a data sets intended for ambient seismic tomography in the Australian continent. Source S1, located off the northern part of Australia's west coast, is strong year round. This case example suggests that a similar understanding of noise (back azimuth, relative strength, and seasonal variability of dominant sources) in other large areas of continental crust should be gained prior to undertaking short term deployments (less than 1 year) for seismic structure determinations.

The results of this study may be interpreted in terms of wave activity in the Southern Ocean and West Pacific and the overall wave climate of these oceans. The seasonality of *P* wave and surface wave sources (Figure 2) has a logical interpretation in view of the elevated storminess expected in the winter season, which occurs in Q1 for Northern Hemisphere sources and Q3 for those in the Southern Hemisphere. Source P1, in the South Atlantic region, is strong year round, with a slight reduction in Q2, the Southern Hemisphere autumn. Both P1 (South Atlantic) and P2 (Kerguelen) are located in the Southern Ocean and are strong noise sources during the Southern Hemisphere winter. The observation that source P1 remains strong in the summer may be due to the enhanced seismic noise due to the combined presence of summer storms, and of the Antarctic Peninsula and South American coastlines, which facilitate seismic noise generation from reflected swells [*Ardhuin et al*., 2011]. In contrast, there are no extended coastlines in the vicinity of Kerguelen.

Ongoing work will focus on multiple weaker sources, some of which are just evident in Figure 1, and also investigate frequency dependent relationships between observed seismic noise sources and wave activity. This study has identified the location and variability of dominant, *P* and higher-mode surface wave, sources of seismic noise toward a fundamental understanding of the seismic noise (microseism) wavefield over many years.

6. Conclusions

From the analysis of a long duration (2000–2012) of seismic array data from WRA, Northern Territory, Australia, we identify three dominant *P* wave sources and three extended regions of dominant surface wave (higher-mode) sources. The three *P* wave sources are the South Atlantic, Kerguelen, and Philippine Sea regions. While some sources are strong year round, the general seasonal pattern shows the *P* wave sources being dominant in the winter quarter for their location. The interannual variation indicates a disruption to the seasonal pattern approximately once every 5 years and will be further analyzed as data spanning ongoing years become available.

Acknowledgments
We thank Richard Aster, an anonymous reviewer, and the Editor for their insightful comments that have strengthened this contribution. Technical staff at WRA, Tennant Creek; Armando Arcidiaco and Chris Tarlowski, RSES, ANU, for their assistance with the extraction and formatting of data; and Brian Kennett for his key role in the long-running operation of WRA. WRA data may be obtained from the IRIS Data Management System [http://www.iris.edu/dms]. Use of open source computer code is acknowledged [http://www.python.org], and the analysis algorithm may be obtained from the authors. The research was funded by the Australian Research Council (DP110103677).

The Editor thanks Richard Aster and an anonymous reviewer for their assistance evaluating this paper.

References

Ardhuin, F., E. Stutzmann, M. Schimmel, and A. Mangeney (2011), Ocean wave sources of seismic noise, *J. Geophys. Res.*, *116*, C09004, doi:10.1029/2011JC006952.

Aster, R. C., D. E. McNamara, and P. D. Bromirski (2010), Global trends in extremal microseism intensity, *Geophys. Res. Lett.*, *37*, L14303, doi:10.1029/2010GL043472.

Berger, J., P. Davis, and G. Ekstrom (2004), Ambient Earth noise: A survey of the Global Seismographic Network, *J. Geophys. Res.*, *109*, B11307, doi:10.1029/2004JB003408.

Beyreuther, M., R. Barsch, L. Krischer, T. Megies, Y. Behr, and J. Wassermann (2010), ObsPy: A Python toolbox for seismology, *Seismol. Rev. Lett.*, *81*(3), 530–533, doi:10.1785/gssrl.81.3.530.

Boning, C. W., A. Dispert, M. Visbeck, S. R. Rintoul, and F. U. Schwarzkopf (2008), The response of the Antarctic Circumpolar Current to recent climate change, *Nat. Geosci.*, *1*(12), 864–869, doi:10.1038/ngeo362.

Campillo, M., and A. Paul (2003), Long-range correlations in the diffuse seismic coda, *Science*, *299*(5606), 547–549, doi:10.1126/science.1078551.

Canadell, J. G., C. Le Quere, M. R. Raupach, C. B. Field, E. T. Buitenhuis, P. Ciais, T. J. Conway, N. P. Gillett, R. A. Houghton, and G. Marland (2007), Contributions to accelerating atmospheric CO(2) growth from economic activity, carbon intensity, and efficiency of natural sinks, *Proc. Natl. Acad. Sci. U. S. A.*, *104*(47), 18,866–18,870, doi:10.1073/pnas.0702737104.

Capon, J. (1969), High-resolution frequency-wavenumber spectrum analysis, *Proc. IEEE*, *57*(8), 1408–1418, doi:10.1109/proc.1969.7278.

Cessaro, R. K. (1994), Sources of primary and secondary microseisms, *Bull. Seismol. Soc. Am.*, *84*(1), 142–148.

Durrant, T., D. Greenslade, M. Hemer, and C. Trenham (2013), A 30-year global wave hindcast focuses on the South Pacific, 13th International wave forecasting and hindcasting workshop, Banff, Canada, Oct 2013. [Available at http://www.waveworkshop.org/13thWaves/Papers/Durrant.pdf.]

Euler, G. G., D. A. Wiens, and A. A. Nyblade (2014), Evidence for bathymetric control on the distribution of body waves microseism sources from temporary seismic arrays in Africa, *Geophys. J. Int.*, doi:10.1093/gji/ggu1105, in press.

Ewing, W. M., W. S. Jardetzky, and F. Press (1957), *Elastic Waves in Layered Media*, McGraw-Hill, New York.

Featherstone, W. (1997), A novel method to improve the performance of Capon's minimum variance estimator, Antennas and Propagation, Tenth International Conference on (Conf. Publ. No. 436), *1*, 332–335, doi:10.1049/cp:19970264.

Gerstoft, P., P. M. Shearer, N. Harmon, and J. Zhang (2008), Global P, PP, and PKP wave microseisms observed from distant storms, *Geophys. Res. Lett.*, *35*, L23306, doi:10.1029/2008GL036111.

Google Earth (2013), Google Earth Pro 7.1, 2013. Terrain Primary Database, November 2013. [Available at http://www.google.com/earth.]

Gruber, N., et al. (2009), Oceanic sources, sinks, and transport of atmospheric CO_2, *Global Biogeochem. Cycles*, *23*, GB1005, doi:10.1029/2008GB003349.

Hanson, J. L., B. A. Tracey, H. L. Tolman, and R. D. Scott (2009), Pacific hindcast performance of three numerical wave models, *J. Atmos. Oceanic Technol.*, *26*, 1614–1633, doi:10.1175/2009JTECHO650.1.

Harmon, N., C. Rychert, and P. Gerstoft (2010), Distribution of noise sources for seismic interferometry, *Geophys. J. Int.* , *183*(3), 1470–1484, doi:10.1111/j.1365-246X.2010.04802.x.

Hasselmann, K. (1963), A statistical analysis of the generation of microseisms, *Rev. Geophys.*, *1*(2), 177–210, doi:10.1029/RG001i002p00177.

Hemer, M. A. (2010), Historical trends in Southern Ocean storminess: Long-term variability of extreme wave heights at Cape Sorell, Tasmania, *Geophys. Res. Lett.*, *37*, L18601, doi:10.1029/2010GL044595.

Hemer, M. A., J. A. Church, and J. R. Hunter (2010), Variability and trends in the directional wave climate of the Southern Hemisphere, *Int. J. Climatol.*, *30*(4), 475–491, doi:10.1002/joc.1900.

Hillers, G., N. Graham, M. Campillo, S. Kedar, M. Landès, and N. Shapiro (2012), Global oceanic microseism sources as seen by seismic arrays and predicted by wave action models, *Geochem., Geophys., Geosyst.*, *13*, Q01021, doi:10.1029/2011GC003875.

Kennett, B. L. N., E. R. Engdahl, and R. Buland (1995), Constraints on seismic velocities in the Earth from travel times, *Geophys. J. Int.*, *122*, 108–124, doi:10.1111/j.1365-246X.1995.tb03540.

Koper, K. D., B. de Foy, and H. Benz (2009), Composition and variation of noise recorded at the Yellowknife Seismic Array, 1991–2007, *J. Geophys. Res.*, *114*, B10310, doi:10.1029/2009JB006307.

Koper, K. D., K. Seats, and H. Benz (2010), On the composition of Earth's short-period seismic noise field, *Bull. Seismol. Soc. Am.*, *100*(2), 606–617, doi:10.1785/0120090120.

Kvaerna, T., and F. Ringdal (1986), Stability of various f-k estimation techniques, NORSAR Scientific Report, 1(86/87), 29-40.

Kvaerna, T., and D. Doornbos (1986), An integrated approach to slowness analysis with array and three-component stations, NORSAR Semiannual Technical Summary, 2(85/86), 60–69.

Lacoss, R. T., E. J. Kelly, and M. N. Toksoz (1969), Estimation of seismic noise structure using arrays, *Geophysics*, *34*(1), 21–38, doi:10.1190/1.1439995.

Landès, M., F. Hubans, N. M. Shapiro, A. Paul, and M. Campillo (2010), Origin of deep ocean microseisms by using teleseismic body waves, *J. Geophys. Res.*, *115*, B05302, doi:10.1029/2009JB006918.

Le Quere, C., et al. (2007), Saturation of the Southern Ocean CO_2 sink due to recent climate change, *Science*, *316*(5832), 1735–1738, doi:10.1126/science.1136188.

Le Quere, C., et al. (2009), Trends in the sources and sinks of carbon dioxide, *Nat. Geosci.*, *2*(12), 831–836, doi:10.1038/ngeo689.

Longuet-Higgins, M. S. (1950), A theory of the origin of microseisms, *Philos. Trans. R. Soc. London, Ser. A*, *243*, 1–35, doi:10.1098/rsta.1950.0012.

Obrebski, M. J., F. Ardhuin, E. Stutzmann, and M. Schimmel (2012), How moderate sea states can generate loud seismic noise in the deep ocean, *Geophys. Res. Lett.*, *39*, L11601, doi:10.1029/2012GL051896.

Poli, P., M. Campillo, H. Pedersen, and the LAPNET Working Group (2012), Body-wave imaging of Earth's mantle discontinuities from ambient seismic noise, *Science*, *338*(6110), 1063–1065, doi:10.1126/science.1228194.

Prieto, G. A., J. F. Lawrence, and G. C. Beroza (2009), Anelastic Earth structure from the coherency of the ambient seismic field, *J. Geophys. Res.*, *114*, B07303, doi:10.1029/2008JB006067.

Rhie, J., and B. Romanowicz (2006), A study of the relation between ocean storms and the Earth's hum, *Geochem., Geophys., Geosyst.*, *7*, Q10004, doi:10.1029/2006GC001274.

Romanowicz, B. (2008), Using seismic waves to image Earth's internal structure, *Nature*, *451*(7176), 266–268, doi:10.1038/nature06583.

Shapiro, N. M., and M. Campillo (2004), Emergence of broadband Rayleigh waves from correlations of the ambient seismic noise, *Geophys. Res. Lett.*, *31*, L07614, doi:10.1029/2004GL019491.

Stutzmann, E., G. Roult, and L. Astiz (2000), GEOSCOPE station noise levels, *Bull. Seismol. Soc. Am.*, *90*, 690–701, doi:10.1785/0119990025.

Stutzmann, E., M. Schimmel, G. Patau, and A. Maggi (2009), Global climate imprint on seismic noise, *Geochem., Geophys., Geosyst.*, *10*, Q11004, doi:10.1029/2009GC002619.

Tkalčić, H., N. Rawlinson, P. Arroucau, A. Kumar, and B. L. N. Kennett (2012), Multistep modelling of receiver-based seismic and ambient noise data from WOMBAT array: Crustal structure beneath southeast Australia, *Geophys. J. Int.*, *189*(3), 1681–1700, doi:10.1111/j.1365-246X.2012.05442.x.

Traer, J., P. Gerstoft, P. D. Bromirski, and P. M. Shearer (2012), Microseisms and hum from ocean surface gravity waves, *J. Geophys. Res.*, *117*, B11307, doi:10.1029/2012JB009550.

Wax, M., T. J. Shan, and T. Kailath (1984), Spatio-temporal spectral-analysis by eigenstructure methods, *IEEE Trans. Acoust. Speech Signal Process.*, *32*(4), 817–827, doi:10.1109/tassp.1984.1164400.

Young, I. R., S. Zieger, and A. V. Babanin (2011), Global trends in wind speed and wave height, *Science*, *332*(6028), 451–455, doi:10.1126/science.1197219.

Zhang, J., P. Gerstoft, and P. M. Shearer (2010), Resolving P-wave travel-time anomalies using seismic array observations of oceanic storms, *Earth Planet. Sci. Lett.*, *292*(3-4), 419–427, doi:10.1016/j.epsl.2010.02.014.